The Astronomical Journal, 155:84 (10pp), 2018 February https://doi.org/10.3847/1538-3881/aaa3e4

The K2-HERMES Survey. I. Planet-candidate Properties from K2 Campaigns 1–3

Robert A. Wittenmyer[1,2], Sanjib Sharma[3], Dennis Stello[3,4,5], Sven Buder[6,23], Janez Kos[3], Martin Asplund[7], Ly Duong[7], Jane Lin[7], Karin Lind[6,8], Melissa Ness[6], Tomaz Zwitter[9], Jonathan Horner[1], Jake Clark[1], Stephen R. Kane[10], Daniel Huber[3,11,12,13], Joss Bland-Hawthorn[3], Andrew R. Casey[14], Gayandhi M. De Silva[3,15], Valentina D'Orazi[16], Ken Freeman[7], Sarah Martell[4], Jeffrey D. Simpson[15], Daniel B. Zucker[15,17,18], Borja Anguiano[17,19], Luca Casagrande[20], James Esdaile[4], Marc Hon[4], Michael Ireland[20], Prajwal R. Kafle[21], Shourya Khanna[3], J. P. Marshall[22], Mohd Hafiz Mohd Saddon[4], Gregor Traven[9], and Duncan Wright[4,15]

[1] University of Southern Queensland, Computational Engineering and Science Research Centre, Toowoomba, Queensland 4350, Australia; rob.w@usq.edu.au
[2] Australian Centre for Astrobiology, University of New South Wales, Sydney, NSW 2052, Australia
[3] Sydney Institute for Astronomy, School of Physics, University of Sydney, NSW 2006, Australia
[4] School of Physics, University of New South Wales, Sydney, NSW 2052, Australia
[5] Stellar Astrophysics Centre, Department of Physics and Astronomy, Aarhus University, DK-8000 Aarhus C, Denmark
[6] Max Planck Institute for Astronomy (MPIA), Koenigstuhl 17, D-69117 Heidelberg, Germany
[7] Research School of Astronomy & Astrophysics, Australian National University, ACT 2611, Australia
[8] Department of Physics and Astronomy, Uppsala University, Box 516, SE-751 20 Uppsala, Sweden
[9] Faculty of Mathematics and Physics, University of Ljubljana, Jadranska 19, 1000 Ljubljana, Slovenia
[10] Department of Earth Sciences, University of California, Riverside, CA 92521, USA
[11] Institute for Astronomy, University of Hawai'i, 2680 Woodlawn Drive, Honolulu, HI 96822, USA
[12] SETI Institute, 189 Bernardo Avenue, Mountain View, CA 94043, USA
[13] Stellar Astrophysics Centre, Department of Physics and Astronomy, Aarhus University, Ny Munkegade 120, DK-8000 Aarhus C, Denmark
[14] Monash Centre for Astrophysics, School of Physics & Astronomy, Monash University, Clayton 3800, Victoria, Australia
[15] Australian Astronomical Observatory, 105 Delhi Road, North Ryde, NSW 2113, Australia
[16] INAF Osservatorio Astronomico di Padova, vicolo dell'Osservatorio 5, I-35122, Padova, Italy
[17] Department of Physics & Astronomy, Macquarie University, Sydney, NSW 2109, Australia
[18] Research Centre in Astronomy, Astrophysics & Astrophotonics, Macquarie University, Sydney, NSW 2109, Australia
[19] Department of Astronomy, University of Virginia, Charlottesville, VA 22904-4325, USA
[20] Research School of Astronomy & Astrophysics, Australian National University, Cotter Road, Weston Creek, ACT 2611 Australia
[21] International Centre for Radio Astronomy Research (ICRAR), The University of Western Australia, 35 Stirling Highway, Crawley, WA 6009, Australia
[22] Academia Sinica, Institute of Astronomy and Astrophysics, Taipei 10617, Taiwan
Received 2017 October 17; revised 2017 December 14; accepted 2017 December 18; published 2018 January 24

Abstract

Accurate and precise radius estimates of transiting exoplanets are critical for understanding their compositions and formation mechanisms. To know the planet, we must know the host star in as much detail as possible. We present first results from the K2-HERMES project, which uses the HERMES multi-object spectrograph on the Anglo-Australian Telescope to obtain $R \sim 28000$ spectra of up to 360 stars in one exposure. This ongoing project aims to derive self-consistent spectroscopic parameters for about half of K2 target stars. We present complete stellar parameters and isochrone-derived masses and radii for 46 stars hosting 57 K2 candidate planets in Campaigns 1–3. Our revised host-star radii cast severe doubt on three candidate planets: EPIC 201407812.01, EPIC 203070421.01, and EPIC 202843107.01, all of which now have inferred radii well in excess of the largest known inflated Jovian planets.

Key words: planets and satellites: fundamental parameters – stars: fundamental parameters – techniques: spectroscopic

1. Introduction

A little over two decades ago, the first planets were discovered orbiting Sun-like stars (Mayor & Queloz 1995; Butler & Marcy 1996; Marcy & Butler 1996), and humanity entered the exoplanet era. Those first planets revolutionized our understanding of planet formation and offered a tantalizing hint to the uniqueness of the architecture of our solar system.

In the years that followed, the number of known exoplanets grew—and the surprises continued to come. Some systems contained planets moving on highly eccentric orbits (e.g., Tamuz et al. 2008; Wittenmyer et al. 2009; Kane et al. 2016). Others had multiple planets on highly compact orbits, far closer to their host stars than the distance between Mercury and the Sun (e.g., Lissauer et al. 2011; Campante et al. 2015; Gillon et al. 2017), or planets on highly inclined orbits (e.g., Triaud et al. 2010; Addison et al. 2013; Huber et al. 2013).

However, the techniques used to discover these myriad planets are all strongly biased—toward more massive planets, and typically toward planets with short orbital periods (e.g., O'Toole et al. 2009; Kipping & Sandford 2016; Vanderburg et al. 2016b). To begin searching for true solar system analogues requires either a search for massive long-period planets (e.g., Bedell et al. 2015; Endl et al. 2016; Wittenmyer et al. 2016, 2017) or a search for small worlds analogous to the terrestrial planets (e.g., Wittenmyer et al. 2011; Howard et al. 2012; Swift et al. 2015).

The first real information on the frequency of planets that resemble the solar system's rocky worlds came from the *Kepler* spacecraft (Borucki et al. 2010), which stared continuously at a single patch of the sky for just over four years. By observing

[23] Fellow of the International Max Planck Research School for Astronomy & Cosmic Physics at the University of Heidelberg.

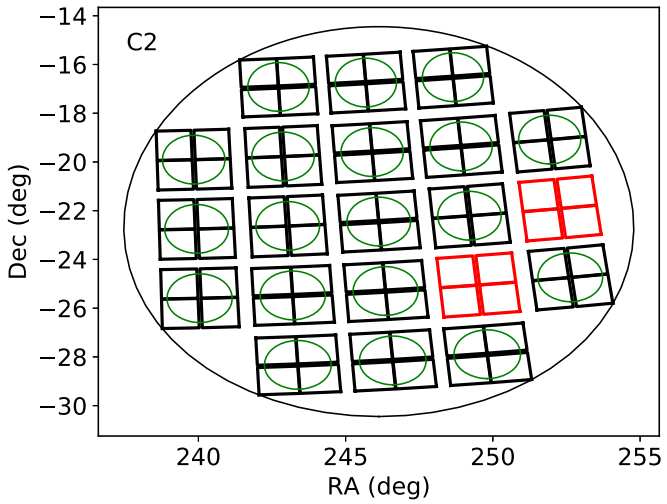

Figure 1. The *Kepler* field of view and the layout of its CCD modules, overlaid with the HERMES field of view (green circles). The red modules are inoperative.

over 100,000 stars, *Kepler* discovered an unprecedented number of planets (Coughlin et al. 2016)—including objects as small as the planet Mercury (Barclay et al. 2013). From *Kepler*'s great census, it has become clear that small planets are common—which might be the first hint that our solar system is far from unique.

In 2014, the second of *Kepler*'s four reaction wheels, used to orient the spacecraft and keep it pointing at its target field of view, failed. As a result, the first phase of *Kepler*'s mission came to an end, and the spacecraft was repurposed to carry out the K2 survey (Howell et al. 2014). The telescope was re-oriented to point in the plane of the ecliptic—a position it could maintain without requiring the use of the broken reaction wheels.

To avoid pointing directly at the Sun, the K2 mission points at any given patch of the ecliptic for a period of about 80 days. At the end of that observing cycle, it pivots further away from the Sun, to point at a new field, and repeat the process. Where the original *Kepler* survey searched for planets out to orbital periods of around one year, K2 can find only those planets with the shortest orbital periods. However, to counterbalance this, through the full K2 mission, the spacecraft will be able to observe a diverse multitude of community-selected stars, and thereby yield a new treasure trove of short-period planets to add to the original survey's grand census (e.g., Crossfield et al. 2016; Vanderburg et al. 2016a).

To fully understand the nature of the planets found orbiting those stars, it is critically important that the stars themselves are well characterized and understood (e.g., Huber et al. 2014; Ren et al. 2016; Petigura et al. 2017). As a result, there is a need for the target stars to be observed spectroscopically from the ground. With such a large number of stars to be targeted, it would be grossly inefficient to observe them one at a time—but fortunately, in Australia, the 2dF/HERMES instrument on the Anglo-Australian Telescope is ideally suited to such a survey.

Built to perform "Galactic Archaeology" (e.g., Kos et al. 2017; Martell et al. 2017; Traven et al. 2017), the 2dF/HERMES instrument allows observers to obtain high-quality and high-resolution ($R \sim 28{,}000$) spectra of several hundred stars in a single observation—typically of around an hour's duration. Observations with HERMES allow the abundances of a number of species in the target stars to be determined, as well as enabling us to obtain relatively precise values for the stellar parameters (mass, radius, and age)—information critical to the understanding of the plethora of planets that will be found by the K2 mission.

In this paper, we present the first observations from the K2-HERMES survey. In Section 2, we describe the observing setup for our survey and give more detail on the 2dF/HERMES instrument. In Section 3, we describe how the stellar parameters have been calculated from the HERMES spectra, before detailing the physical properties of the *K*2 planet candidates orbiting those stars in Section 4. Finally, in Section 5, we present our conclusions and discuss our plans for future work.

2. Observations and Data Analysis

The observations were obtained with the 3.9 m Anglo-Australian Telescope located at Siding Spring Observatory in Australia. We use the High Efficiency and Resolution Multi-Element Spectrograph (HERMES), which can obtain spectra of up to 360 science targets simultaneously (Barden et al. 2010; Brzeski et al. 2011; Heijmans et al. 2012; Sheinis et al. 2015).

2.1. Observational Strategy

A single 2dF/HERMES exposure covers most of a *Kepler* CCD module (Figure 1), enabling relatively efficient observations of K2 fields. Our objective is simply to gather spectra for as many K2 targets as possible, without introducing biases driven by the relative probability of hosting a planet. As with the related TESS-HERMES program (Sharma et al. 2018), we favor bright stars to obtain targets of most interest for asteroseismic and exoplanetary science. Owing to fiber "cross talk" in the instrument, we follow the procedure implemented by the GALAH survey (Martell et al. 2017), where the fields are chosen such that the brightest and faintest stars observed do not differ in brightness by more than three magnitudes. Balancing this against the desire for the most efficient use of the 360 HERMES science fibers results in a strategy whereby we observe each *Kepler* CCD module twice: once as a bright visit ($10 < V < 13$) and again as a faint visit ($13 < V < 15$). Bright visits consist of a single 30-minute exposure, while faint visits consist of three 30-minute exposures. In the bright visits, HERMES typically observes all of the available bright stars in a single pass. The total number of stars per 2dF field in this range is typically less than 360, so we can observe all of them in one 2dF pointing. In the faint visits, the total number of stars per 2dF field is greater than 400 but the number of *K*2 targets is 210 on average. This means all K2 targets lying within a 2dF circle can be observed in just one telescope pointing (consisting of a "bright" and a "faint" exposure).

2.2. Raw Reduction

The K2-HERMES survey uses the same instrument as the GALAH survey (De Silva et al. 2015; Martell et al. 2017) and follows a similar observing strategy. Hence, we use the same reduction pipeline as GALAH to perform the data reduction from the raw CCD images to the final calibrated spectra. The procedure, described fully in Kos et al. (2017) and Sharma et al. (2018), is in brief: (1) raw reduction is performed with a custom IRAF-based pipeline, (2) four basic parameters ($T_{\rm eff}$, log g, [Fe/H], and radial velocity) and continuum normalization are calculated with a custom pipeline "GUESS" by

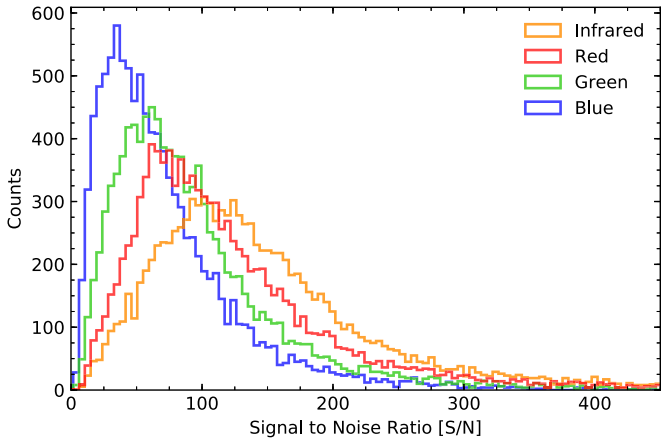

Figure 2. Signal to noise per resolution element for the four HERMES bandpasses.

matching the observed normalized spectra to synthetic templates. A grid of AMBRE synthetic spectra is used for this purpose de Laverny et al. (2012). Figure 2 shows a histogram of the signal-to-noise (S/N) for our K2-HERMES spectra in each of the four HERMES bandpasses.

3. Determination of Stellar Parameters

The spectroscopic stellar parameters have been estimated with a combination of classical spectrum synthesis for a representative reference set of stars and a data-driven approach to propagate the high-fidelity parameter information with higher precision onto all of the stars in the K2-HERMES survey. The method is identical to that used by the TESS-HERMES survey (Sharma et al. 2018) and is briefly outlined as follows. First, we use the spectrum synthesis code Spectroscopy Made Easy (SME) by Piskunov & Valenti (2017) to analyse the reference set. This training set includes samples of stars with external parameter estimates, *Gaia* benchmark FGK stars, and stars with asteroseismic information from K2 Campaign 1 (Stello et al. 2017). Next, we use these SME results as training labels of the training set as input for *The Cannon* (Ness et al. 2015) to propagate the analysis to all stars. As shown by Sharma et al. (2018), the comparison with benchmark stars shows trends and systematic offsets for the hottest/coolest dwarfs and turnoff/subgiant stars of our survey, which are however below 250 K (for $T_{\rm eff}$) and 0.25 dex (for $\log g$). Similar shortcomings have been noted by Torres et al. (2012) as well as Bensby et al. (2014). With new data provided by *Gaia*, we will however be able to overcome such shortcomings of purely spectroscopic analyses in future data releases for the joint GALAH/K2/TESS pipeline for HERMES. A more detailed explanation will be given by S. Buder et al. (2018, in preparation), who include, e.g., *Gaia* parallaxes to constrain $\log g$ for the training set of the GALAH Data Release 2.

Derived stellar properties such as mass, radius, and age are then computed via the Bayesian Stellar Parameters estimator (BSTEP), described fully in Sharma et al. (2018). The input observables J, $J-K_s$, $T_{\rm eff}$, $\log g$, [Fe/H] are brought to bear on a grid of about 5×10^6 points in [Fe/H], age, and initial mass, outputting the intrinsic parameters [Fe/H], age, initial mass, distance, $E(B-V)$, and their probabilities. The output is then used to compute other derived parameters, like stellar mass and radius, which are functions of the intrinsic parameters. In Table 1, we report our results for the 46 planet-candidate host stars observed by K2-HERMES during C1–C3. Figure 3 gives a comparison of our derived radii and masses with those obtained by the empirical method of Torres et al. (2010). There is good agreement within uncertainties, and no systematic trends are evident.

While none of the planet-candidate host stars discussed here are a priori known to be binaries, five are flagged as possible binaries from the t-SNE classification as described in Traven et al. (2017). Closer inspection of the spectra reveals that four of these stars display evidence for a second set of lines: EPIC 201407812, 202634963, 202688980, and 203753577. These stars have been marked as binaries in Table 1, and the presence of a weak secondary set of lines may have affected *The Cannon* analysis. Hence, we caution that those stellar parameters, while not obviously erroneous, are potentially unreliable. The fifth, EPIC 206024342, is flagged but the spectrum S/N is too low to visually detect any features of a second set of lines.

Huber et al. (2016) presented a catalog of stellar parameters for 138,600 stars in K2 campaigns 1–8. For the vast majority of those stars, parameters were derived from photometry; here, we compare those results with our spectroscopically derived parameters. Figure 4 shows the difference in $\log g$ derived here with that from Huber et al. (2016), as a function of the difference in $T_{\rm eff}$ from the two works. The center and right panels of Figure 4 show similar comparisons, but for [Fe/H] and the derived stellar radii, respectively. No systematic trends are apparent, apart from the expected anticorrelation between $\log g$ (panel a) and the stellar radius (panel c). That is, stars for which we obtain a smaller $\log g$ will have a larger derived radius. The median parameter offsets, in the sense of (this work—H16), are as follows: $\Delta T_{\rm eff} = -39 \pm 287$ K, $\Delta \log g = -0.06 \pm 0.54$ dex, Δ[Fe/H] $= -0.025 \pm 0.392$, and $\Delta R_* = 0.04 \pm 2.38\,R_\odot$.

The right panels of Figure 4 give a comparison of our derived stellar radii with those of H16. Some stars do exhibit significant differences in derived radii, which is mainly due to the difference in $\log g$. Huber et al. (2016) measured $\log g$ from photometry and proper motions, introducing substantial uncertainty (as evidenced by the large error bars in Figure 4). We find four stars with $\log g$ (H16)—$\log g$ (this work) < -0.7. These are all red giants in H16 but we classify them as dwarfs. We also find two stars with large differences in the opposite direction: $\log g$ (H16)—$\log g$ (this work) > 0.7. They are EPIC 201516974 and EPIC 203070421. The first was classified as a low-luminosity giant in H16, but our results place it in the red clump region with $\log g = 2.66 \pm 0.12$. The second was a hot dwarf but now sits in an odd position in the ($\log g$, $T_{\rm eff}$) plane. In our spectroscopic pipeline, it is flagged as being too far away from the training set, and so we caution the reader that the results for that star may be suspect.

4. Planet-candidate Parameters

Table 2 gives the properties of the 57 planet candidates from C1–C3 for which the K2-HERMES program has obtained spectra of their host stars. The planet data (orbital period and R_p/R_*) have been obtained from the NASA Exoplanet Archive. We derived the planetary radii by multiplying R_p/R_* by the stellar radii obtained by our grid-based modeling as described above. Uncertainties in the planetary radii result from the propagated uncertainties in R_* and R_p/R_*; for those

Table 1
Parameters for Planet-candidate Host Stars

EPIC ID	$T_{\rm eff}$	log g	[Fe/H]	Mass ($M_{\odot}$)	Radius ($R_{\odot}$)
201155177	4695 ± 200	4.56 ± 0.20	−0.17 ± 0.26	0.69 ± 0.05	0.66 ± 0.04
201291843	4146 ± 200	4.62 ± 0.20	−0.47 ± 0.26	0.59 ± 0.04	0.59 ± 0.04
201393098	5625 ± 125	3.90 ± 0.20	−0.25 ± 0.10	0.97 ± 0.12	1.75 ± 0.39
201403446	6110 ± 76	4.06 ± 0.16	−0.42 ± 0.08	0.94 ± 0.07	1.38 ± 0.28
201407812[a]	5951 ± 125	4.03 ± 0.15	−1.02 ± 0.06	0.82 ± 0.05	1.70 ± 0.24
201516974	4912 ± 45	2.66 ± 0.12	−0.60 ± 0.05	1.07 ± 0.21	8.19 ± 1.60
201546283	5256 ± 60	4.54 ± 0.14	+0.22 ± 0.06	0.90 ± 0.03	0.87 ± 0.04
201606542	5355 ± 73	4.63 ± 0.15	+0.24 ± 0.07	0.93 ± 0.03	0.90 ± 0.05
201855371	4440 ± 200	4.60 ± 0.20	−0.17 ± 0.26	0.65 ± 0.05	0.63 ± 0.04
201912552	4180 ± 200	4.62 ± 0.20	−0.69 ± 0.26	0.51 ± 0.05	0.50 ± 0.05
202634963[a]	6385 ± 125	4.30 ± 0.20	−0.59 ± 0.10	0.96 ± 0.06	1.16 ± 0.22
202675839	5719 ± 125	4.07 ± 0.20	+0.46 ± 0.10	1.13 ± 0.13	1.53 ± 0.36
202688980[a]	6456 ± 117	4.29 ± 0.18	−0.55 ± 0.10	1.00 ± 0.06	1.18 ± 0.21
202821899	6024 ± 125	3.91 ± 0.20	+0.30 ± 0.10	1.42 ± 0.20	2.10 ± 0.60
202843107	7493 ± 65	3.69 ± 0.15	−0.19 ± 0.06	1.93 ± 0.16	3.29 ± 0.63
203070421	6157 ± 125	2.79 ± 0.20	−0.18 ± 0.10	2.82 ± 0.54	11.16 ± 3.94
203518244	6205 ± 125	3.80 ± 0.20	−0.09 ± 0.10	1.37 ± 0.21	2.21 ± 0.58
203533312	6400 ± 45	4.01 ± 0.12	−0.15 ± 0.05	1.27 ± 0.11	1.83 ± 0.29
203753577[a]	6171 ± 47	4.01 ± 0.11	+0.05 ± 0.05	1.29 ± 0.11	1.84 ± 0.28
203771098	5644 ± 40	4.35 ± 0.11	+0.50 ± 0.05	1.03 ± 0.02	1.12 ± 0.12
203826436	5379 ± 125	4.55 ± 0.20	0.00 ± 0.10	0.87 ± 0.05	0.84 ± 0.06
203867512	6367 ± 47	3.86 ± 0.12	−0.15 ± 0.05	1.39 ± 0.14	2.23 ± 0.43
203929178	6820 ± 64	4.34 ± 0.12	−0.62 ± 0.05	1.09 ± 0.03	1.20 ± 0.14
204221263	5643 ± 40	4.30 ± 0.11	+0.34 ± 0.05	1.03 ± 0.02	1.18 ± 0.14
205050711	7072 ± 113	3.92 ± 0.17	−0.05 ± 0.09	1.62 ± 0.17	2.25 ± 0.56
205071984	5351 ± 125	4.50 ± 0.20	+0.01 ± 0.10	0.88 ± 0.05	0.86 ± 0.07
205111664	5577 ± 125	4.14 ± 0.20	−0.19 ± 0.10	0.91 ± 0.08	1.38 ± 0.47
205570849	5950 ± 125	4.27 ± 0.20	−0.14 ± 0.10	0.98 ± 0.07	1.18 ± 0.24
205924614	4310 ± 200	4.61 ± 0.20	−0.11 ± 0.26	0.65 ± 0.06	0.63 ± 0.05
205944181	5250 ± 125	4.48 ± 0.20	+0.05 ± 0.10	0.86 ± 0.04	0.83 ± 0.05
205950854	5422 ± 125	4.36 ± 0.20	−0.17 ± 0.10	0.84 ± 0.05	0.83 ± 0.08
205957328	5295 ± 76	4.74 ± 0.15	+0.13 ± 0.07	0.88 ± 0.03	0.84 ± 0.04
206024342	5801 ± 125	4.20 ± 0.20	−0.24 ± 0.10	0.90 ± 0.06	1.14 ± 0.28
206026136	4548 ± 200	4.58 ± 0.20	−0.10 ± 0.26	0.69 ± 0.05	0.66 ± 0.04
206038483	5597 ± 77	4.12 ± 0.16	+0.26 ± 0.08	1.02 ± 0.06	1.35 ± 0.27
206049452	4447 ± 200	4.59 ± 0.20	−0.27 ± 0.26	0.65 ± 0.05	0.63 ± 0.05
206055981	4544 ± 200	4.58 ± 0.20	−0.30 ± 0.26	0.65 ± 0.06	0.63 ± 0.05
206082454	5573 ± 125	4.79 ± 0.20	+0.11 ± 0.10	0.95 ± 0.05	0.93 ± 0.07
206096602	4561 ± 200	4.58 ± 0.20	−0.18 ± 0.26	0.69 ± 0.06	0.66 ± 0.05
206103150	5392 ± 125	4.08 ± 0.20	+0.34 ± 0.10	1.00 ± 0.08	1.39 ± 0.37
206114630	5097 ± 44	4.53 ± 0.11	+0.06 ± 0.05	0.82 ± 0.02	0.78 ± 0.02
206125618	5351 ± 125	4.37 ± 0.20	+0.04 ± 0.10	0.88 ± 0.05	0.87 ± 0.08
206135682	4838 ± 42	4.74 ± 0.20	−0.12 ± 0.10	0.73 ± 0.03	0.70 ± 0.03
206245553	5819 ± 42	4.35 ± 0.11	+0.08 ± 0.05	1.02 ± 0.03	1.12 ± 0.13
206311743	5146 ± 125	4.04 ± 0.20	−0.42 ± 0.10	0.93 ± 0.09	2.38 ± 0.42
206417197	5111 ± 125	4.61 ± 0.20	0.00 ± 0.10	0.81 ± 0.04	0.77 ± 0.04

Note.
[a] Double-lined spectroscopic binary.

planet candidates from Vanderburg et al. (2016a) without published uncertainties in R_p/R_*, we adopted the median fractional uncertainty of 0.0025 obtained by Crossfield et al. (2016). Figure 5 shows our newly derived planet radii against published values (Table 2).

For the majority of planets, our newly derived radii agree with the published values, though we do find that for six planet candidates, our results show radii that are more than $>3\sigma$ larger than the published values. Of these, five orbit somewhat evolved stars with radii in the range 1.9–8 $R_{\odot}$, resulting in larger inferred planetary radii, turning some potentially terrestrial worlds into gas giants. The most dramatic change is candidate super-Earth EPIC 203070421.01 (Vanderburg et al. 2016a), now approaching three Jupiter radii. Given that the largest inflated planets are $\sim$2 $R_{\rm Jup}$, our revised host-star parameters suggest that this candidate is a false positive.

The various catalogs of K2 planet candidates contain some fraction of stars with spectroscopically derived parameters and others with photometrically derived parameters only. In Figure 6, we reprise Figure 5 comparing our results with published values, but showing only those for which the published values were derived from spectroscopic measurements. Notably, all of the candidates identified in Vanderburg et al. (2016a) had only photometric host-star radii, and that

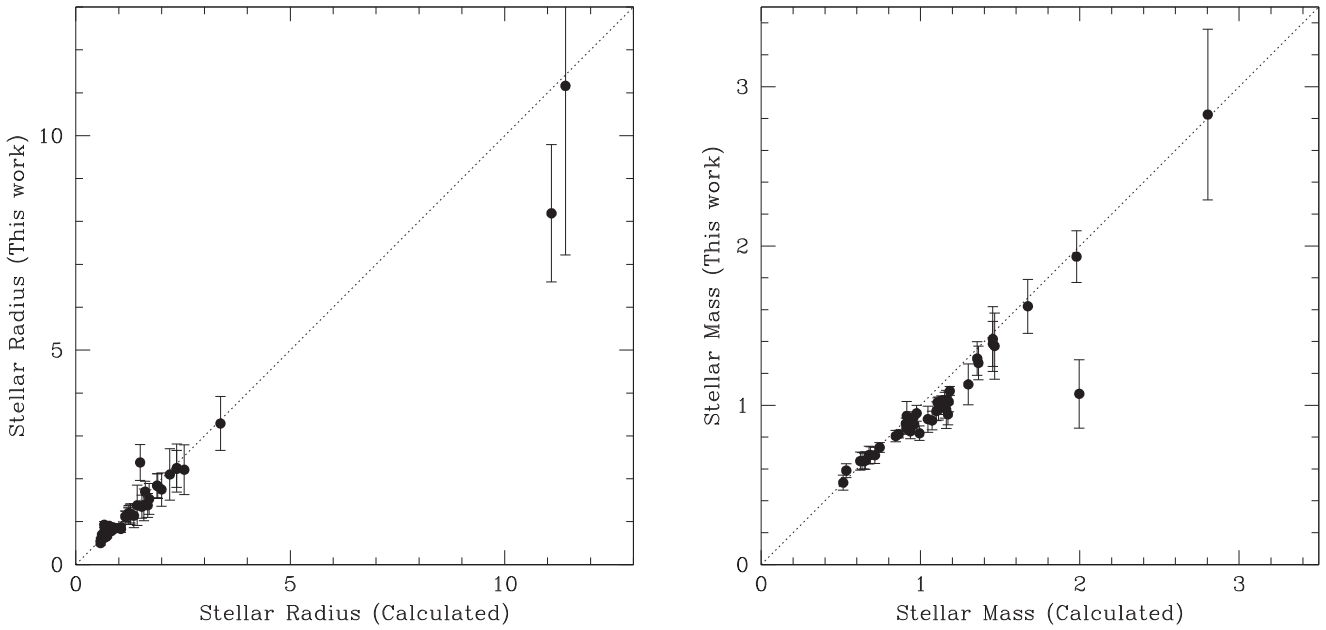

Figure 3. Comparison of our derived stellar radii (left) and masses (right) with those estimated from the empirical relations of Torres et al. (2010).

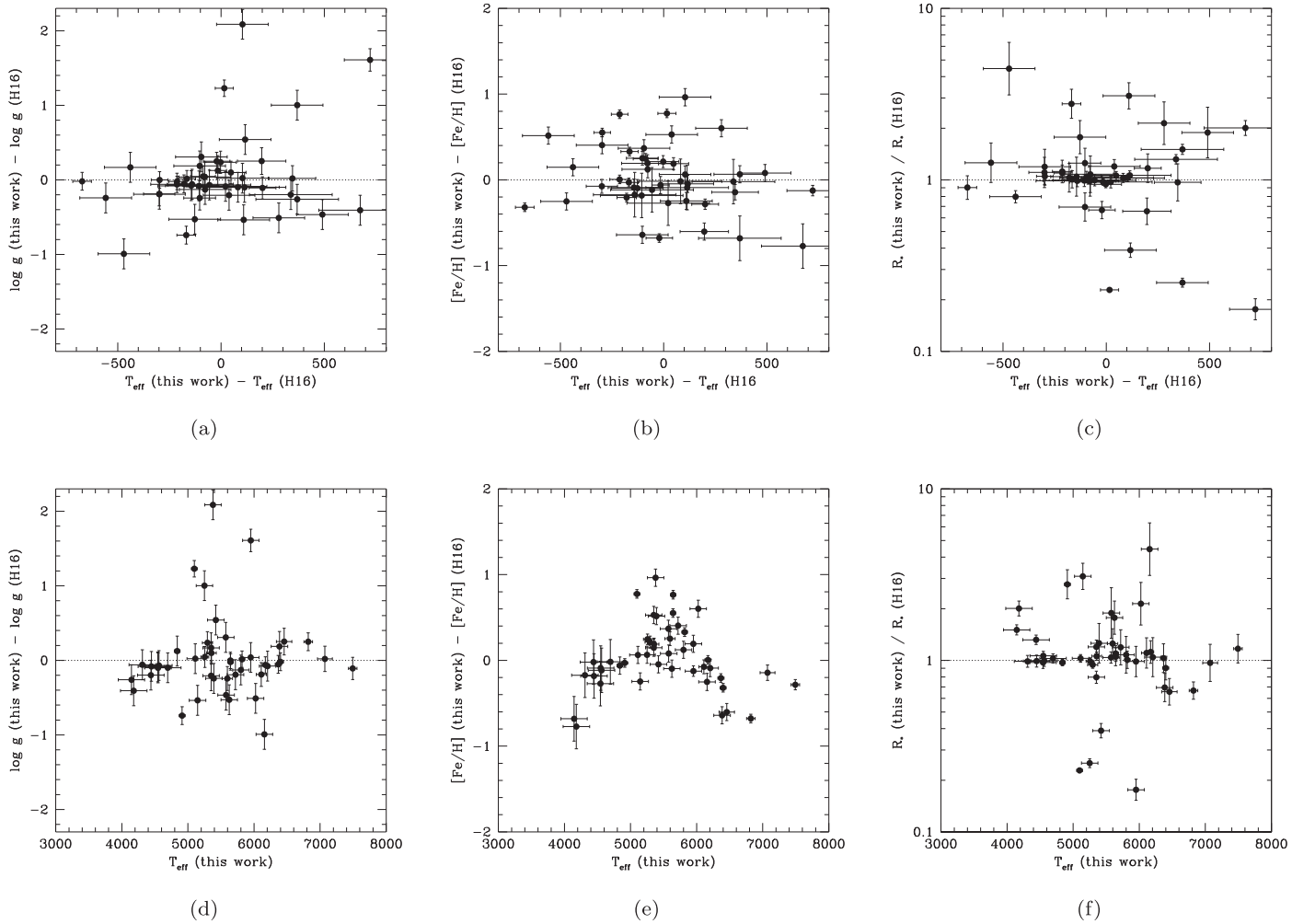

Figure 4. Comparison of our spectroscopic stellar parameters with those of Huber et al. (2016), as a function of the differences in $T_{\rm eff}$ (top row) and the $T_{\rm eff}$ derived herein (bottom row). Error bars shown are those from this work. Panels (a), (d): log g, panels (b), (e): [Fe/H], panels (c), (f): stellar radius.

Table 2
Planet-candidate Properties

EPIC ID	K2 ID	P (Days)	a (au)	R_p/R_*	R_p ($R_\oplus$)	$S_{\rm inc}$ $F_\oplus$	$T_{\rm eq}$ (K) Hot Dayside	$T_{\rm eq}$ (K) Well-mixed
201155177	K2-42b	6.68796 ± 0.00093	0.061	0.0304 ± 0.0028[a]	2.19 ± 0.25	47.229	868.5	730.3
201291843		40.70206194	0.194	0.00536 ± 0.00028[b]	0.34 ± 0.03	2.556	418.9	352.2
201393098	K2-7b	28.6777 ± 0.0086	0.182	0.0177 ± 0.0018[a]	3.38 ± 0.84	84.638	1004.8	845.0
201403446	K2-46b	19.1541 ± 0.0041	0.140	0.0145 ± 0.001[a]	2.18 ± 0.47	125.074	1107.9	931.6
201407812[c]		2.8268121	0.037	0.4560[d]	84.68 ± 12.00	2419.735	2323.5	1953.8
201516974		36.762337	0.221	0.03712[d]	33.21 ± 6.84	719.553	1715.8	1442.8
201546283	K2-27b	6.771315 ± 0.000079	0.068	0.0474 ± 0.00093[a]	4.53 ± 0.24	115.165	1085.3	912.6
201606542		0.444372 ± 0.000042	0.011	0.0136 ± 0.002[e]	1.33 ± 0.21	4796.510	2757.0	2318.3
201855371	K2-17b	17.9654 ± 0.0017	0.116	0.029 ± 0.0025[a]	2.00 ± 0.22	9.692	584.5	491.5
201912552	K2-18b	32.9418 ± 0.0021	0.161	0.0517 ± 0.0021[a]	2.82 ± 0.32	2.453	414.6	348.6
202634963[c]		28.707623	0.181	0.2136[d]	27.05 ± 5.14	61.455	927.6	780.0
202675839		15.4715 ± 0.0036	0.127	0.044 ± 0.075[a]	7.35 ± 12.64	144.466	1148.5	965.8
202688980[c]		1.45566370	0.025	0.02958 ± 0.00036[b]	3.82 ± 0.67	3438.517	2536.9	2133.2
202821899		4.4743465	0.060	0.03229[d]	7.40 ± 2.18	1449.133	2044.0	1718.8
202843107		2.1989041	0.041	0.6032[d]	216.57 ± 41.66	17909.266	3832.4	3222.7
203070421		1.7359447	0.040	0.02551[d]	31.08 ± 11.40	100522.547	5898.9	4960.3
203518244		0.84112570	0.019	0.01098[d]	2.65 ± 0.92	17425.977	3806.3	3200.7
203533312		0.17566 ± 0.000183	0.007	0.0248 ± 0.001[e]	4.95 ± 0.82	113835.766	6085.2	5117.0
203753577[c]		3.4007758	0.050	0.06863[d]	13.78 ± 2.16	1886.993	2183.5	1836.1
203771098.1	K2-24c	42.36301 ± 0.00072	0.241	0.05913 ± 0.00053[a]	7.25 ± 0.75	19.848	699.3	588.0
203771098.2	K2-24b	20.88526 ± 0.00042	0.150	0.04264 ± 0.00081[a]	5.23 ± 0.55	50.962	885.1	744.3
203826436.1	K2-37b	4.44118 ± 0.00074	0.050	0.0174 ± 0.0015[a]	1.60 ± 0.18	210.138	1261.3	1060.7
203826436.2	K2-37c	6.42973 ± 0.00043	0.065	0.0276 ± 0.0018[a]	2.54 ± 0.25	128.305	1115.0	937.6
203826436.3	K2-37d	14.0919 ± 0.0015	0.109	0.0271 ± 0.0021[a]	2.50 ± 0.27	45.069	858.4	721.8
203867512		28.465633	0.203	0.1642[d]	39.98 ± 7.70	175.975	1206.6	1014.6
203929178		1.153886 ± 0.000028	0.022	0.53 ± 0.23[a]	69.23 ± 31.17	5693.021	2877.7	2419.8
204221263.1	K2-38b	4.01628 ± 0.00044	0.050	0.01329 ± 0.00099[a]	1.72 ± 0.24	508.436	1573.1	1322.8
204221263.2	K2-38c	10.56098 ± 0.00081	0.095	0.0195 ± 0.0014[a]	2.52 ± 0.35	140.087	1139.7	958.4
205050711		4.30221683	0.061	0.02613 ± 0.00074[b]	6.41 ± 1.62	3029.473	2457.8	2066.8
205071984.1	K2-32b	8.99213 ± 0.00015	0.081	0.0556 ± 0.0014[a]	5.24 ± 0.43	86.520	1010.4	849.6
205071984.2	K2-32c	20.6602 ± 0.0016	0.141	0.0326 ± 0.0021[a]	3.07 ± 0.31	28.538	765.7	643.9
205071984.3	K2-32d	31.7154 ± 0.0020	0.188	0.0371 ± 0.0031[a]	3.50 ± 0.40	16.115	663.8	558.2
205111664		15.937378	0.120	0.02135[d]	3.22 ± 1.16	125.627	1109.1	932.6
205570849		16.8580 ± 0.0011	0.128	0.047 ± 0.057[a]	6.04 ± 7.43	96.813	1039.2	873.8
205924614	K2-55b	2.849258 ± 0.000033	0.034	0.0552 ± 0.0013[a]	3.81 ± 0.30	107.097	1065.7	896.2
205944181		2.475527 ± 0.000083	0.034	0.38 ± 0.35[a]	34.55 ± 31.89	412.831	1493.3	1255.7
205950854		15.854120	0.116	0.02208[d]	2.00 ± 0.29	41.132	839.0	705.5
205957328		14.353347	0.111	0.02383[d]	2.19 ± 0.25	40.436	835.4	702.5
206024342.1		14.6370 ± 0.0021	0.113	0.0249 ± 0.0015[a]	3.09 ± 0.79	107.512	1066.8	897.0
206024342.2		0.91165670	0.018	0.01593[d]	1.98 ± 0.58	4354.620	2691.2	2263.0
206026136	K2-57b	9.0063 ± 0.0013	0.075	0.0308 ± 0.0028[a]	2.23 ± 0.25	30.411	778.0	654.2
206038483	K2-60b	3.002627 ± 0.000018	0.041	0.06191 ± 0.00035[a]	9.12 ± 1.80	959.652	1843.9	1550.5
206049452		14.454495	0.101	0.02923[d]	2.01 ± 0.23	14.350	644.8	542.2
206055981		20.643928	0.128	0.03129[d]	2.16 ± 0.24	9.585	582.9	490.2
206082454.1		14.317001	0.113	0.01714[d]	1.73 ± 0.29	57.351	911.7	766.6
206082454.2		29.626402	0.184	0.03282[d]	3.32 ± 0.36	21.749	715.4	601.6
206096602.1	K2-62b	6.67202 ± 0.00028	0.061	0.0271 ± 0.0017[a]	1.95 ± 0.18	47.468	869.6	731.2
206096602.2	K2-62c	16.1966 ± 0.0012	0.111	0.0269 ± 0.0019[a]	1.94 ± 0.19	14.549	647.0	544.1
206103150.1	WASP-47b	4.159221 ± 0.000015	0.051	0.10214 ± 0.0003[a]	15.54 ± 4.08	627.497	1658.1	1394.3
206103150.2	WASP-47d	9.03164 ± 0.00064	0.085	0.026 ± 0.0015[a]	3.96 ± 1.06	223.155	1280.4	1076.7
206103150.3	WASP-47e	0.789518 ± 0.000060	0.017	0.01344 ± 0.00088[a]	2.04 ± 0.55	5751.909	2885.1	2426.0
206114630		7.4448754	0.070	2.65 ± 0.23[d]	2.65 ± 0.23	75.689	977.2	821.7
206125618	K2-64b	6.53044 ± 0.00067	0.065	0.0259 ± 0.0017[a]	2.47 ± 0.27	132.337	1123.6	944.9
206135682		5.0258310	0.052	0.01961[d]	1.49 ± 0.20	91.188	1023.7	860.9
206245553	K2-73b	7.49543 ± 0.00059	0.075	0.021 ± 0.0012[a]	2.56 ± 0.33	223.737	1281.3	1077.4
206311743		4.31444335	0.051	0.03877 ± 0.00040[b]	10.06 ± 1.79	1404.529	2028.1	1705.4
206417197		0.442094 ± 0.000086	0.011	0.0138 ± 0.001[e]	1.15 ± 0.10	3122.265	2476.4	2082.4

Notes.
[a] Crossfield et al. (2016).
[b] Barros et al. (2016).
[c] Double-lined spectroscopic binary star.
[d] Vanderburg et al. (2016a).
[e] Adams et al. (2016).

catalog was the source of all of the discrepant results discussed above. The remaining planets shown in Figure 6 are in excellent agreement with the published spectroscopic results.

As noted in Section 3, four stars in this sample are found to be binaries. We thus caution that the following (as-yet unconfirmed) planet candidates may be false positives: EPIC 201407812, 202634963, 202688980, and 203753577.

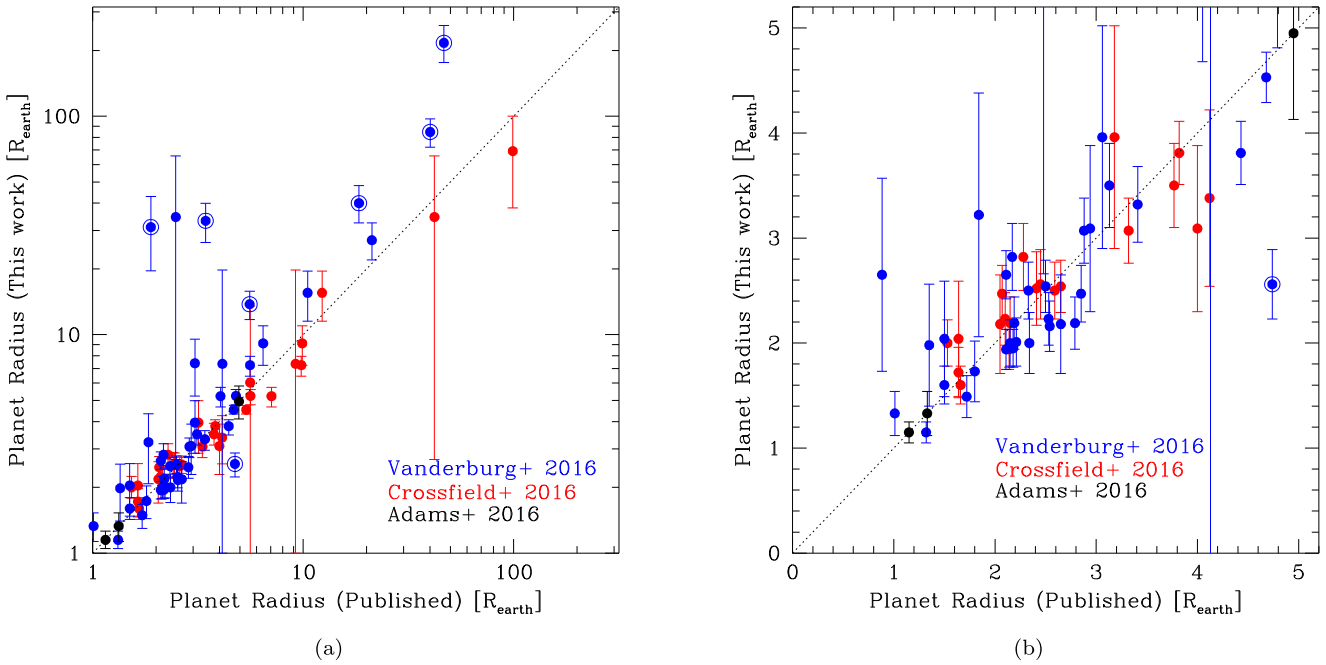

Figure 5. Left panel: radii of K2 planet candidates from C1–C3, as derived in this work using K2-HERMES spectra, compared with the radii as reported in their discovery works. Blue: Vanderburg et al. (2016a)—Red: Crossfield et al. (2016)—Black: Adams et al. (2016). Error bars on previously published values are omitted for clarity. Right panel: the same, but for planets smaller than 5 $R_{\oplus}$. For the majority of planets, our results agree with the published radii, though we now find six planets with radii more than 3σ larger than their published values, all from the Vanderburg et al. (2016a) catalog. Planets differing from their published values by more than 3σ are shown as encircled points.

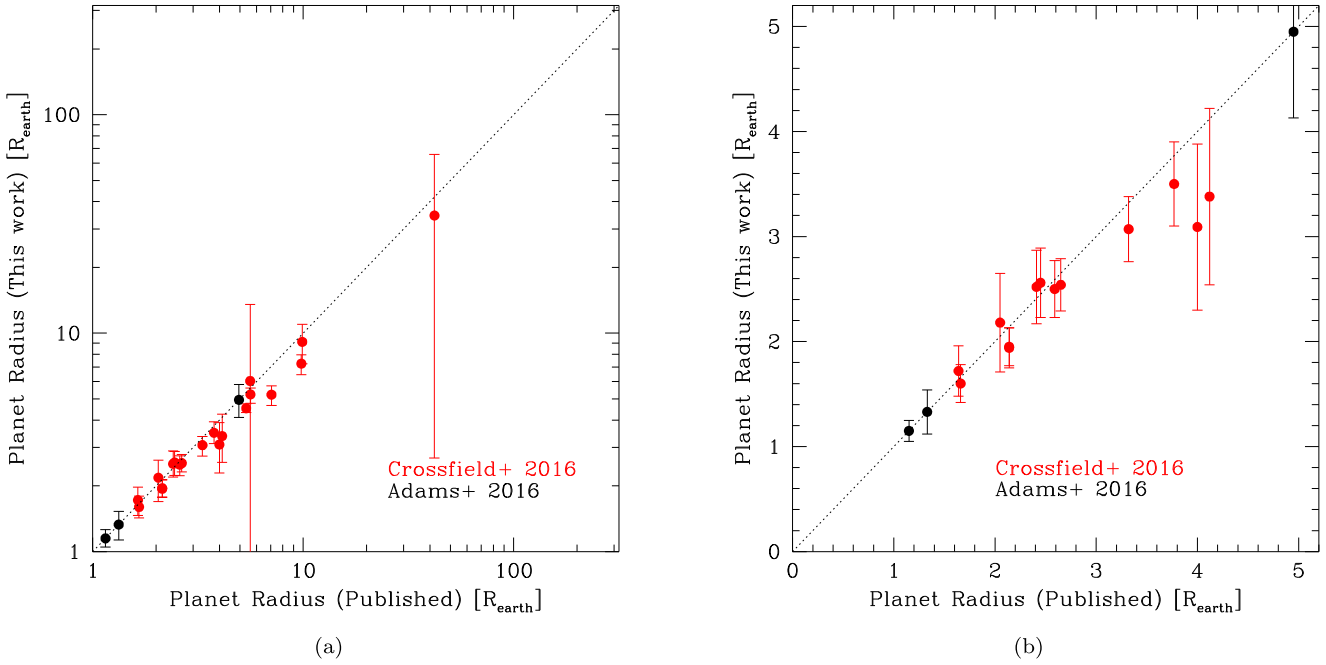

Figure 6. The same as Figure 5, but only showing those planets for which the previously published radii were derived using spectroscopic measurements of their host stars.

Most of the 57 planet candidates examined here remain within the range of reasonable planet radii (i.e., smaller than a few tens of Earth radii). However, EPIC 202843107.01 now has a radius of 216.6 $R_{\oplus}$ (approximately 2 solar radii). That candidate has an exceptionally deep transit ($R_p/R_* = 0.6032$), again unphysically large for a planet, particularly given that the host star appears to be a main-sequence A star (Table 1). We thus strongly suspect EPIC 202843107.01 is a false positive. Similarly, EPIC 201407812 hosts a candidate 84.7 $R_{\oplus}$ planet, (nearly eight Jupiter radii); given that the host is now confirmed as a binary, this candidate also appears to be a false positive.

Our revised stellar parameters bring to light some interesting individual planets in this sample. One metal-poor star hosts a candidate giant planet: EPIC 206311743 ([Fe/H] $= -0.42 \pm$

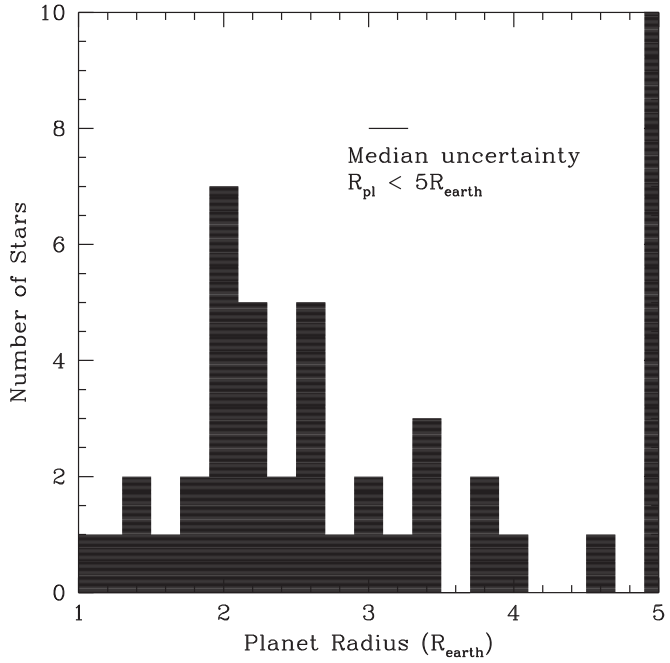

Figure 7. Histogram of our derived radii for 38 K2 planet candidates smaller than 5 $R_\oplus$. The median uncertainty in radius for these planets is shown as a horizontal bar (0.27 $R_\oplus$). This distribution peaks at ~2.0 $R_\oplus$ with a secondary peak near 2.6 $R_\oplus$.

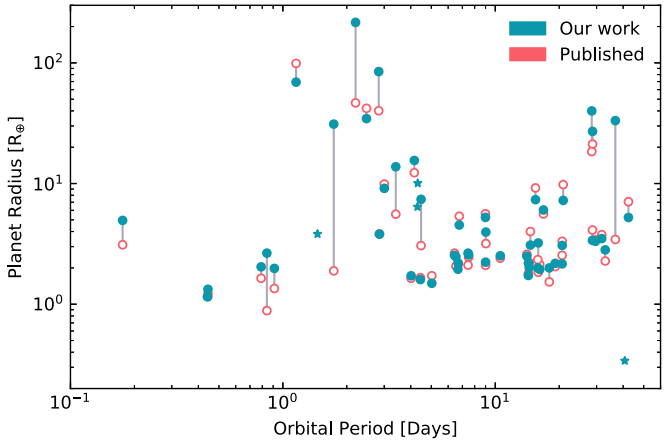

Figure 8. Planet radius vs. orbital period for the 57 planets examined here. Filled circles indicate our newly derived radii, connected to open circles denoting the previously published radii.

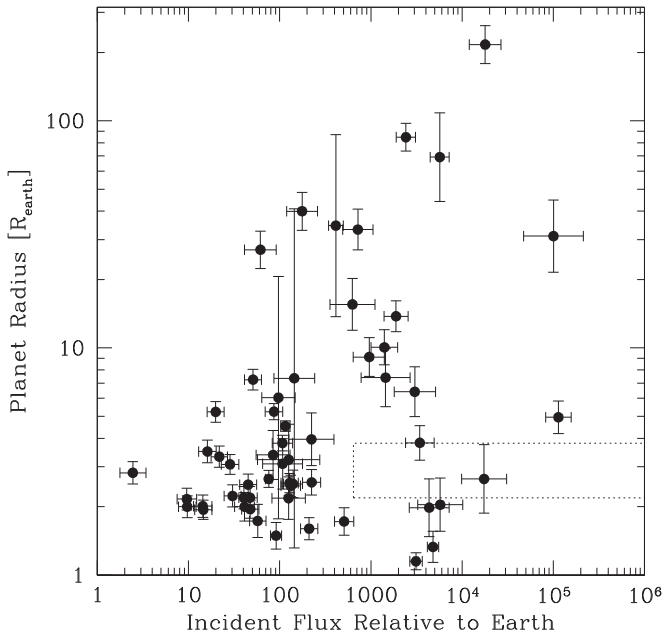

Figure 9. Planet radii vs. incident flux for our 57 planets. The dashed lines enclose the "hot super-earth desert" postulated by Lundkvist et al. (2016), denoting planets receiving more than 650 times Earth's incident flux, and radii from 2.2 to 3.8 $R_\oplus$. We find only one planet falling in this region: EPIC 203518244b.

0.10). A second star, EPIC 202634963, also hosts a candidate planet but we confirm it to be a double-lined spectroscopic binary and hence is likely to be a false positive. Such planets are rare by virtue of the well-known planet-metallicity correlation (Gonzalez 1997; Fischer & Valenti 2005), whereby giant planets have difficulty forming by core accretion from metal-poor protoplanetary disks. While both remain candidates, if they were to be confirmed, they would be extremely interesting counterexamples.

Close-in planets orbiting evolved stars are also known to be rare, with only 12 known within 0.5 au from the various radial velocity surveys of so-called "retired A stars" (e.g., Bowler et al. 2010; Jones et al. 2015; Wittenmyer et al. 2015). Our sample contains two giants (log $g < 3.5$), each hosting one planet candidate. They are EPIC 201516974 and EPIC 203070421, neither of which is flagged as a binary star. Caution is warranted, however, as giant stars are intrinsically more noisy (due to granulation), and hence the false-positive rate of detecting transit signals is higher (Sliski & Kipping 2014).

The California-*Kepler* Survey (CKS) team have noted that *Kepler* planets exhibit a gap in their radius distribution (Fulton et al. 2017), with planets of 1.5–2.0 $R_\oplus$ apparently depleted by more than a factor of two. In light of this finding, we examine the radius distribution for the 38 small ($R_p < 5\,R_\oplus$) *K*2 planets featured herein (Figure 7). As perhaps expected with the low numbers involved, no compelling pattern is yet evident; future papers extending this work to further *K*2 campaigns will provide the necessary data to fill in this distribution. Figure 8 shows the planetary radii versus orbital period, with lines connecting the updated radii to their previously published counterparts.

The incident flux levels and equilibrium temperatures of the planet candidates are also shown in Table 2. For completeness, we give two values of equilibrium temperature: "hot dayside" and "well-mixed," corresponding to re-radiation over 2π and 4π steradians, respectively. The former would be most suitable for close-in planets presumed to be tidally locked. Figure 9 shows the relation of the planet radii and their incident fluxes for the 57 planet candidates considered here. Lundkvist et al. (2016) identified a "hot super-Earth desert": a lack of planets between 2.2–3.8 $R_\oplus$ receiving incident flux more than 650 times that of Earth. The envelopes of these planets have been stripped by photoevaporation. From the *Kepler* planet sample for which the host stars have been characterized by asteroseismology, Lundkvist et al. (2016) found no planets in that range; in our sample of K2 planet candidates, we find one object falling within the dashed rectangle in Figure 9. That candidate, EPIC 203518244b, orbits a star we characterize as a slightly evolved F subgiant ($T_{\rm eff} = 6205 \pm 125$ K, log $g = 3.8 \pm 0.2$, and $M_* = 1.37 \pm 0.21\,M_\odot$). Our parameters for this star are in excellent agreement with those of Huber et al. (2016), who derived $T_{\rm eff} = 6349$ K, log $g = 3.9$, and $M_* = 1.42\,M_\odot$.

Table 3
Habitable Zone Boundaries for Planet-candidate Host Stars

EPIC ID	Inner HZ (au) Optimistic	Inner HZ (au) Conservative	Outer HZ (au) Optimistic	Outer HZ (au) Conservative
201155177	0.33	0.42	0.78	0.82
201291843	0.25	0.32	0.60	0.63
201393098	1.27	1.60	2.84	2.99
201403446	1.13	1.43	2.50	2.64
201407812	1.34	1.70	2.98	3.14
201516974	4.67	5.91	10.74	11.33
201546283	0.56	0.71	1.27	1.34
201606542	0.59	0.75	1.34	1.41
201855371	0.29	0.37	0.68	0.72
201912552	0.20	0.26	0.48	0.51
202634963	1.03	1.30	2.26	2.39
202675839	1.15	1.45	2.56	2.70
202688980	1.06	1.34	2.34	2.46
202821899	1.68	2.13	3.73	3.93
202843107	3.78	4.79	8.26	8.71
203070421	9.29	11.76	20.56	21.69
203518244	1.87	2.37	4.13	4.36
203533312	1.62	2.05	3.57	3.76
203753577	1.53	1.94	3.40	3.58
203771098	0.81	1.03	1.82	1.92
203826436	0.56	0.71	1.27	1.34
203867512	1.95	2.47	4.31	4.54
203929178	1.18	1.49	2.59	2.73
204221263	0.85	1.08	1.91	2.01
205050711	2.33	2.95	5.10	5.38
205071984	0.58	0.73	1.31	1.38
205111664	1.02	1.30	2.30	2.42
205570849	0.93	1.18	2.08	2.19
205924614	0.28	0.36	0.67	0.71
205944181	0.53	0.68	1.21	1.28
205950854	0.57	0.72	1.29	1.36
205957328	0.54	0.69	1.23	1.30
206024342	0.88	1.11	1.96	2.07
206026136	0.33	0.42	0.77	0.81
206038483	0.96	1.22	2.16	2.28
206049452	0.31	0.39	0.72	0.76
206055981	0.32	0.40	0.74	0.78
206082454	0.65	0.83	1.47	1.55
206096602	0.34	0.43	0.79	0.83
206103150	0.97	1.23	2.20	2.32
206114630	0.47	0.60	1.08	1.14
206125618	0.58	0.73	1.31	1.38
206135682	0.39	0.49	0.90	0.95
206245553	0.84	1.07	1.88	1.99
206311743	1.48	1.87	3.37	3.55
206417197	0.46	0.58	1.05	1.11

Though none of the planet candidates discussed here are even remotely considered habitable, for completeness we show the stellar habitable zone boundaries in Table 3, which may prove relevant for any outer planets subsequently found to reside in these systems.

5. Summary and Conclusion

We note that *K*2 Campaigns 1–3 have more than 100 identified planet host stars (Adams et al. 2016; Crossfield et al. 2016; Vanderburg et al. 2016a), whereas this work currently presents spectroscopically derived stellar properties for 57 planets orbiting 46 stars. The "missed" planet hosts can be accounted for primarily by (1) targets falling on the corners of the *Kepler* CCD modules and hence not currently covered by the K2-HERMES survey, and (2) host stars fainter than the faint limit of the K2-HERMES survey. The 2dF field is two degrees in diameter, for an area of 3.14 square degrees, while a single CCD module has an area of five square degrees. This means that K2-HERMES only observes ∼54% of (assumed uniformly distributed) stars falling on *K*2 detectors. *K*2 targets are skewed in favor of cooler, fainter stars (Huber et al. 2016), but our observed sample contains very few stars cooler than ∼4300 K, and our spectroscopic analysis pipeline is currently not equipped to handle very cool stars. Hence, we expect to miss the coolest targets, accounting for about 25% of the total planet candidates (Crossfield et al. 2016). Those stars are most likely to be characterized by surveys using near-infrared spectroscopy (e.g., Muirhead et al. 2014; Dressing et al. 2017a, 2017b).

The precision of our planetary radii is comparable to the published values. The CKS results permitted a significant improvement in the precision of radii for *Kepler* prime mission KOIs (Johnson et al. 2017), primarily because those objects, as a sample, had very few prior spectroscopic observations. On the other hand, the K2 planet candidates described here are small enough in number, and their host stars are sufficiently bright that the discovery teams have obtained spectra of sufficient resolution and S/N to derive reasonably precise stellar (and hence planetary) radii. The primary value of our work is that we have presented a *fully self-consistent* set of spectroscopic and model-derived parameters for the K2 planet-candidate sample. Applying this uniformly derived set of host-star parameters to the planet-candidate sample thus yields a set of self-consistent planetary properties, which is critically important for informing population studies of small exoplanets. Future papers in this series will extend our analysis to additional K2 campaigns. The K2-HERMES first data release paper (S. Sharma et al. 2018, in preparation) will provide precise stellar parameters for thousands of K2 targets, including those without planet detections, facilitating studies of occurrence rates and planetary properties as functions of host-star properties and their relative position in the Galaxy.

D.S. is supported by Australian Research Council Future Fellowship FT1400147. S.S. is funded by University of Sydney Senior Fellowship made possible by the office of the Deputy Vice Chancellor of Research, and partial funding from Bland-Hawthorn's Laureate Fellowship from the Australian Research Council. S.L.M. acknowledges support from the Australian Research Council through DECRA fellowship DE140100598. L.C. is supported by Australian Research Council Future Fellowship FT160100402. This research has made use of NASA's Astrophysics Data System (ADS), and the SIMBAD database, operated at CDS, Strasbourg, France. This research has also made use of the Exoplanet Orbit Database and the Exoplanet Data Explorer at exoplanets.org (Wright et al. 2011; Han et al. 2014). We thank the Australian Time Allocation Committee for their generous allocation of AAT time, which made this work possible.

Software: SME (Piskunov & Valenti 2017), The Cannon (Ness et al. 2015).

ORCID iDs

Robert A. Wittenmyer https://orcid.org/0000-0001-9957-9304
Sanjib Sharma https://orcid.org/0000-0002-0920-809X
Dennis Stello https://orcid.org/0000-0002-4879-3519
Martin Asplund https://orcid.org/0000-0002-5804-3682
Tomaz Zwitter https://orcid.org/0000-0002-2325-8763
Jonathan Horner https://orcid.org/0000-0002-1160-7970
Stephen R. Kane https://orcid.org/0000-0002-7084-0529
Joss Bland-Hawthorn https://orcid.org/0000-0001-7516-4016
Ken Freeman https://orcid.org/0000-0001-6280-1207
Sarah Martell https://orcid.org/0000-0002-3430-4163
Daniel B. Zucker https://orcid.org/0000-0003-1124-8477
Luca Casagrande https://orcid.org/0000-0003-2688-7511
Michael Ireland https://orcid.org/0000-0002-6194-043X
Prajwal R. Kafle https://orcid.org/0000-0002-3625-9546
Gregor Traven https://orcid.org/0000-0002-1391-9097

References

Adams, E. R., Jackson, B., & Endl, M. 2016, AJ, 152, 47
Addison, B. C., Tinney, C. G., Wright, D. J., et al. 2013, ApJL, 774, L9
Barclay, T., Rowe, J. F., Lissauer, J. J., et al. 2013, Natur, 494, 452
Barden, S. C., Jones, D. J., Barnes, S. I., et al. 2010, Proc. SPIE, 7735, 773509
Barros, S. C. C., Demangeon, O., & Deleuil, M. 2016, A&A, 594, A100
Bedell, M., Meléndez, J., Bean, J. L., et al. 2015, A&A, 581, A34
Bensby, T., Feltzing, S., & Oey, M. S. 2014, A&A, 562, A71
Borucki, W. J., Koch, D., Basri, G., et al. 2010, Sci, 327, 977
Bowler, B. P., Johnson, J. A., Marcy, G. W., et al. 2010, ApJ, 709, 396
Brzeski, J., Case, S., & Gers, L. 2011, Proc. SPIE, 8125, 812504
Butler, R. P., & Marcy, G. W. 1996, ApJL, 464, L153
Campante, T. L., Barclay, T., Swift, J. J., et al. 2015, ApJ, 799, 170
Coughlin, J. L., Mullally, F., Thompson, S. E., et al. 2016, ApJS, 224, 12
Crossfield, I. J. M., Ciardi, D. R., Petigura, E. A., et al. 2016, ApJS, 226, 7
de Laverny, P., Recio-Blanco, A., Worley, C. C., & Plez, B. 2012, A&A, 544, A126
De Silva, G. M., Freeman, K. C., Bland-Hawthorn, J., et al. 2015, MNRAS, 449, 2604
Dressing, C. D., Newton, E. R., Schlieder, J. E., et al. 2017a, ApJ, 836, 167
Dressing, C. D., Vanderburg, A., Schlieder, J. E., et al. 2017b, AJ, 154, 207
Endl, M., Brugamyer, E. J., Cochran, W. D., et al. 2016, ApJ, 818, 34
Fischer, D. A., & Valenti, J. 2005, ApJ, 622, 1102
Fulton, B. J., Petigura, E. A., Howard, A. W., et al. 2017, AJ, 154, 109
Gillon, M., Triaud, A. H. M. J., Demory, B.-O., et al. 2017, Natur, 542, 456
Gonzalez, G. 1997, MNRAS, 285, 403
Han, E., Wang, S. X., Wright, J. T., et al. 2014, PASP, 126, 827
Heijmans, J., Asplund, M., Barden, S., et al. 2012, Proc. SPIE, 8446, 84460W
Howard, A. W., Marcy, G. W., Bryson, S. T., et al. 2012, ApJS, 201, 15
Howell, S. B., Sobeck, C., Haas, M., et al. 2014, PASP, 126, 398
Huber, D., Bryson, S. T., Haas, M. R., et al. 2016, ApJS, 224, 2
Huber, D., Carter, J. A., Barbieri, M., et al. 2013, Sci, 342, 331
Huber, D., Silva Aguirre, V., Matthews, J. M., et al. 2014, ApJS, 211, 2
Johnson, J. A., Petigura, E. A., Fulton, B. J., et al. 2017, AJ, 154, 108
Jones, M. I., Jenkins, J. S., Rojo, P., Melo, C. H. F., & Bluhm, P. 2015, A&A, 573, A3
Kane, S. R., Wittenmyer, R. A., Hinkel, N. R., et al. 2016, ApJ, 821, 65
Kipping, D. M., & Sandford, E. 2016, MNRAS, 463, 1323
Kos, J., Lin, J., Zwitter, T., et al. 2017, MNRAS, 464, 1259
Lissauer, J. J., Fabrycky, D. C., Ford, E. B., et al. 2011, Natur, 470, 53
Lundkvist, M. S., Kjeldsen, H., Albrecht, S., et al. 2016, NatCo, 7, 11201
Marcy, G. W., & Butler, R. P. 1996, ApJL, 464, L147
Martell, S. L., Sharma, S., Buder, S., et al. 2017, MNRAS, 465, 3203
Mayor, M., & Queloz, D. 1995, Natur, 378, 355
Muirhead, P. S., Becker, J., Feiden, G. A., et al. 2014, ApJS, 213, 5
Ness, M., Hogg, D. W., Rix, H.-W., Ho, A. Y. Q., & Zasowski, G. 2015, ApJ, 808, 16
O'Toole, S. J., Tinney, C. G., Jones, H. R. A., et al. 2009, MNRAS, 392, 641
Petigura, E. A., Howard, A. W., Marcy, G. W., et al. 2017, AJ, 154, 107
Piskunov, N., & Valenti, J. A. 2017, A&A, 597, A16
Ren, A., Fu, J., De Cat, P., et al. 2016, ApJS, 225, 28
Sharma, S., Stello, D., Buder, S., et al. 2018, MNRAS, 473, 2004
Sheinis, A., Anguiano, B., Asplund, M., et al. 2015, JATIS, 1, 035002
Sliski, D. H., & Kipping, D. M. 2014, ApJ, 788, 148
Stello, D., Zinn, J., Elsworth, Y., et al. 2017, ApJ, 835, 83
Swift, J. J., Bottom, M., Johnson, J. A., et al. 2015, JATIS, 1, 027002
Tamuz, O., Ségransan, D., Udry, S., et al. 2008, A&A, 480, L33
Torres, G., Andersen, J., & Giménez, A. 2010, A&ARv, 18, 67
Torres, G., Fischer, D. A., Sozzetti, A., et al. 2012, ApJ, 757, 161
Traven, G., Matijevič, G., Zwitter, T., et al. 2017, ApJS, 228, 24
Triaud, A. H. M. J., Collier Cameron, A., Queloz, D., et al. 2010, A&A, 524, A25
Vanderburg, A., Latham, D. W., Buchhave, L. A., et al. 2016a, ApJS, 222, 14
Vanderburg, A., Plavchan, P., Johnson, J. A., et al. 2016b, MNRAS, 459, 3565
Wittenmyer, R. A., Butler, R. P., Tinney, C. G., et al. 2016, ApJ, 819, 28
Wittenmyer, R. A., Endl, M., Cochran, W. D., Levison, H. F., & Henry, G. W. 2009, ApJS, 182, 97
Wittenmyer, R. A., Horner, J., Mengel, M. W., et al. 2017, AJ, 153, 167
Wittenmyer, R. A., Jones, M., Horner, J., et al. 2017, AJ, 154, 274
Wittenmyer, R. A., Tinney, C. G., Butler, R. P., et al. 2011, ApJ, 738, 81
Wittenmyer, R. A., Wang, L., Liu, F., et al. 2015, ApJ, 800, 74
Wright, J. T., Fakhouri, O., Marcy, G. W., et al. 2011, PASP, 123, 412
Wright, J. T., Marcy, G. W., Howard, A. W., et al. 2012, ApJ, 753, 160